

DOI: 10.1002/adma.200702434

Printable, Flexible, and Stretchable Forms of Ultrananocrystalline Diamond with Applications in Thermal Management**

By *Tae-Ho Kim, Won Mook Choi, Dae-Hyeong Kim, Matthew A. Meitl, Etienne Menard, Hanqing Jiang, John A. Carlisle, and John A. Rogers**

Thin-film diamond has many potential applications in electronics^[1] and optoelectronics,^[2,3] microelectromechanical systems (MEMS),^[4,5] wear-resistant coatings,^[6] thermal management,^[7] and other areas owing to its exceptional electronic, optical, mechanical, chemical/tribological, and thermal properties, respectively.^[8–11] However, challenges in the integration of thin-film diamond with other materials continue to limit its widespread use. Thin-film diamond is most commonly implemented in these systems by directly growing the material on the surfaces of device substrates, where it is used as uniform or lithographically patterned films. This approach places restrictions on the range of applications because all known growth techniques involve relatively high temperatures (>400 °C), vacuum or low pressures, and often other demanding conditions.^[12,13] Integrating thin-film diamond on low-temperature plastics, for example, is not possible. Large-area substrates are also not well-matched to the capabilities of existing deposition techniques, being particularly cost-ineffective when the required diamond coverage is

only sparse. This Communication presents etching and printing techniques that avoid some of these and other limitations. The results demonstrate the ability to integrate films, platelets, ribbons, and other microstructures of ultrananocrystalline diamond (UNCD) with plastic, rubber, glass, and other substrates. Several of these systems provide mechanically bendable and even stretchable structural forms of UNCD. Use as efficient heat spreaders on flexible plastic sheets illustrates a representative application enabled by these approaches.

Figure 1 shows the main processing steps for forming and printing microstructures of thin films of UNCD, which we refer to as μ s-UNCD. First, UNCD is deposited by using hot-filament chemical vapor deposition as a uniform film (400 nm thick) onto a SiO₂ (1 μ m)/Si substrate.^[14,15] This process, which involves continuous renucleation during growth, leads to phase-pure (i.e., no graphitic content) films with nanoscale grain sizes (3–5 nm), atomically abrupt grain boundaries, and other interesting properties.^[15,16] Next, plasma-enhanced chemical vapor deposition (PECVD) creates a layer of SiO₂ (300 nm thick) on top of the UNCD. Photolithography and reactive ion etching (RIE) with a CF₄ plasma defines a pattern in this SiO₂ layer. RIE with an O₂ plasma removes both the photoresist and the exposed UNCD. The SiO₂ on top of and beneath the patterned UNCD is then removed with concentrated hydrofluoric acid (HF 49%). With appropriate pattern geometries, controlled etching allows the UNCD structures to be undercut completely, but in a manner that keeps them tethered to the substrate to prevent their removal into the etching bath. For the case illustrated in Figure 1, these tethers, or “anchors”, consist of narrow regions at the ends of ribbons of UNCD. The printing step involves first contacting a substrate processed in this manner with a slab of an elastomer (i.e., the stamp), to establish a conformal wetting contact with the top surface of the μ s-UNCD through the action of van der Waals forces.^[17] Peeling the stamp away from the substrate at a high rate leads to the selective fracture of the UNCD structures at points of stress concentrations that form at the anchors,^[18] thereby removing these structures from their growth substrate. The stamp, inked with μ s-UNCD in this manner, then delivers these elements to a target substrate, such as plastic, glass, rubber, or a semiconductor wafer, in a room-temperature process that involves contact and then peel-back of the stamp at a slow rate. The transfer is aided

[*] Prof. J. A. Rogers, Dr. T.-H. Kim, Dr. W. M. Choi, D.-H. Kim, Dr. M. A. Meitl, Dr. E. Menard
Department of Materials Science and Engineering
Beckman Institute for Advanced Science and Technology
Frederick Seitz Materials Research Laboratory
University of Illinois at Urbana–Champaign
Urbana, IL 61801 (USA)
E-mail: jrogers@uiuc.edu

Prof. J. A. Rogers
Department of Chemistry, Mechanical Science and Engineering
Beckman Institute for Advanced Science and Technology
University of Illinois at Urbana–Champaign
Urbana, IL 61801 (USA)

Prof. H. Jiang
Department of Mechanical and Aerospace Engineering
Arizona State University, Tempe, AZ 85287 (USA)

Dr. J. A. Carlisle
Advanced Diamond Technologies, Inc.
429 B Weber Road #286, Romeoville, IL 60446 (USA)

[**] This work was supported by the center of Nanoscale Chemical Electrical Mechanical Manufacturing Systems at the University of Illinois, which is funded by National Science Foundation under grant DMI-0328162, and it used facilities in the Center for Microanalysis of Materials in University of Illinois, which is partially supported by the U.S. Department of Energy under grant DEFG02-91-ER45439. Dr. T.-H. Kim acknowledges the Korea Research Foundation Grant KRF-2006-214-D00044, funded by the Korean Government (MOEHRD).

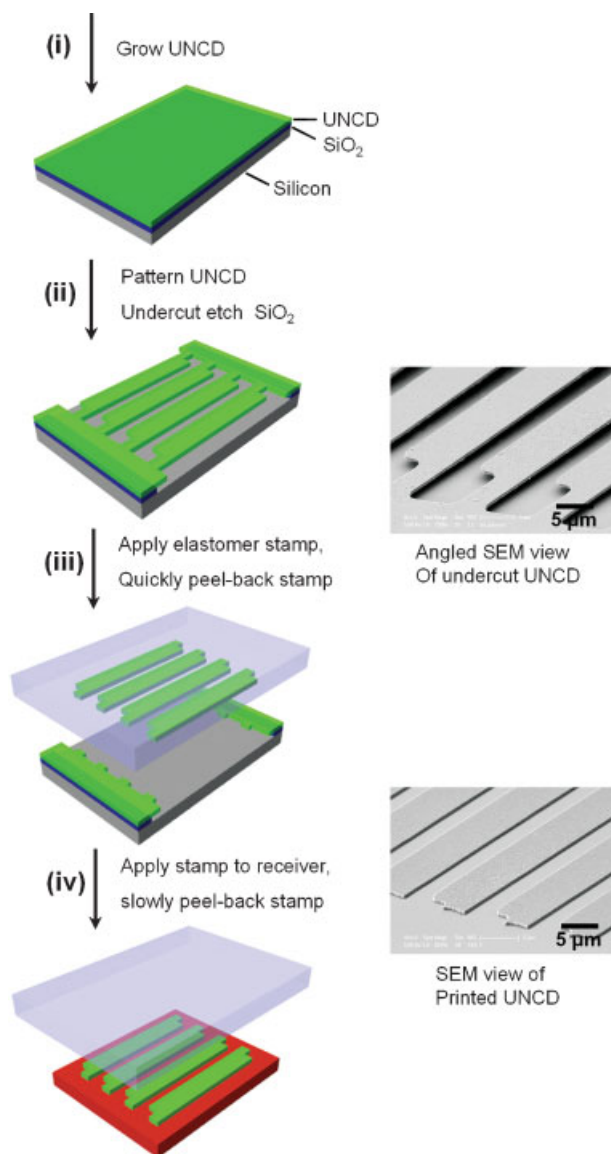


Figure 1. Processing steps for creating microstructures of thin-film ultrananocrystalline diamond and for transferring these elements from a growth substrate to a target substrate by using a printing technique.

either by a thin adhesive layer on the substrate or by an adhesiveless, shear force technique that directs separation at the interface between the stamp and the UNCD.

Figure 2 shows scanning electron microscopy (SEM) and optical microscopy images of diverse classes of thin (400 nm in all cases) diamond microstructures, including membranes (Fig. 2c, square array of 3 μm diameter holes separated by 40 μm to enable SiO₂ undercut etching); interconnected meshes (Fig. 2b, I-shapes with widths and lengths of 25 and 100 μm); and arrays of isolated ribbons (Fig. 2a,d–f, widths and lengths of 10 and 175 μm, respectively), printed with poly(dimethylsiloxane) stamps (PDMS; Dow Corning) onto various substrates, including glass (Fig. 2a–c), GaAs (Fig. 2d), silicon (Fig. 2e), and plastic (polyethyleneterephthalate, PET, with 100 μm

thickness; Fig. 2f). For cases other than the PET and GaAs, a thin, spin-cast layer (ca. 1.0 μm) of benzocyclobutene (BCB, CYCLOTENE 3022-35 Resin, Dow Chemical) served as an adhesive layer to receive the printed μs-UNCD. Adhesiveless printing was used for GaAs, silicon, and PET, in which the transfers were facilitated by (i) the large differences in surface energies of the target substrates (43 mJ m⁻² for PET, 1140 mJ m⁻² for Si, 860 mJ m⁻² for GaAs, and 19.8 mJ m⁻² for the PDMS),^[19,20] (ii) viscoelastic effects associated with low rates for peeling back the stamps,^[21] (iii) the low roughness on the bottom surfaces of the μs-UNCD elements (root-mean-squared (rms) roughness of ca. 1.8 nm, as measured by atomic force microscopy with a standard tip) and the receiving substrates (rms: 0.22 nm for Si, 0.25 nm for GaAs, 0.45 nm for glass and 38 nm for PET), and (iv) shear forces to facilitate crack formation at the PDMS/UNCD interface. The topsides of the UNCD structures exhibit the nanometer-scale roughness characteristic of UNCD, while the undersides are smooth.^[22] The high printing yields (>85% in all cases) and the uniformity of the fracture points associated with the isolated ribbons (Fig. 2a,d, and e) are evidence of well-controlled, repeatable processes.

The results of Figure 2f indicate the ability to bend, without cracking, the μs-UNCD when placed on a thin plastic sheet. In this case, the small thicknesses of both the substrate and the μs-UNCD lead to small strains at the surface for moderately small bend radii. The strain, ϵ , in the diamond is approximately equal to

$$\frac{h_P}{2r} \left[1 - \frac{E_D h_D}{E_P h_P} + \left(\frac{E_D h_D}{E_P h_P} \right)^2 \right] \times 100\%, \quad (1)$$

where E_P and h_P , and E_D and h_D are the modulus and thickness of the PET substrate and diamond, respectively; r is the bending radius. For the bending radius ($r \sim 2$ cm), PET thickness ($h_P \sim 100$ μm), and diamond thickness ($h_D \sim 400$ nm) corresponding to the image of Figure 2f the peak strain in the diamond is $\epsilon \sim 0.17\%$, well below the fracture point. Structural configurations that combine thin, flexible geometries such as these with “wavy” shapes can impart mechanical stretchability to these elements in strategies that are conceptually similar to those recently described for single-crystalline elements of Si, GaAs, and other materials.^[23,24] Figure 3a and b show optical and scanning electron microscopy images of arrays of wavy UNCD ribbons created by transfer printing these elements onto a prestrained ($\sim 4.8\%$ created by heating to 180 °C) substrate of PDMS followed by release of this prestrain.^[25] The distances between the ribbons in this case are sufficiently small that mechanical coupling results in phase coherent buckling patterns. The waves have uniform, periodic structures with wavelengths of 85.2 and 86.3 μm for prestrains of 4.8 and 3.9%, respectively. The prestrain-dependent wavelength values agree well with other experimental observations and accurate models of the mechanics.^[23,26] Figure 3c presents optical images of stretchable diamond ribbons (the sample prepared

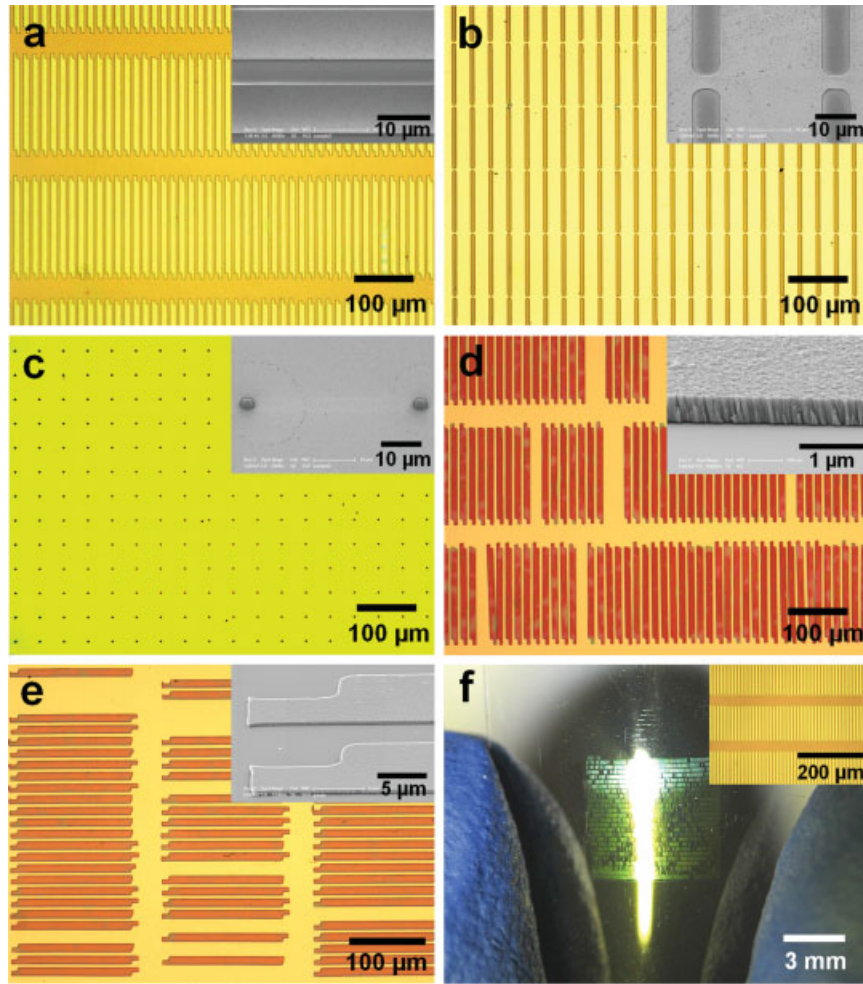


Figure 2. Optical microscopy images and scanning electron microscopy images of transfer-printed UNCD microstructures. a) Isolated ribbons on glass. b) mesh structures on glass. c) Membrane printed on glass. d) Isolated ribbons on GaAs. e) Isolated ribbons on Si. f) Photograph of ribbons on poly(ethylene terephthalate) (PET), in a bent configuration.

with 4.78% prestrain) with various levels of strain at compressed, unperturbed, and stretched states. For applied compressive strains larger than ca. 5%, some cracking of the UNCD was observed (Fig. 3c). We conducted theoretical analysis of the wavy structures, comprising 400 nm thick UNCD film, 30 nm thick SiO₂ film with Young's modulus and Poisson's ratio of 94 GPa and 0.33, respectively, and 4 mm thick PDMS substrate with Young's modulus and Poisson ratio of 2 MPa and 0.48, respectively. If we assume a Poisson's ratio of 0.07 for the diamond, analysis based on the observed buckling wavelengths yields a Young's modulus for the UNCD of 780 GPa, consistent with reports based on conventional mechanical testing techniques.^[23,27] The detailed mechanics of these systems, including the dependence of the stretchability and bendability on thickness and other parameters, can be found in Ref. [26b].

The ability to manipulate thin diamond films in the manner illustrated in Figures 1–3 creates new application possibilities. As one example, we consider the use of printed μs-UNCD as heat spreaders in flexible electronic systems that use low-

temperature plastic substrates. Such a system might represent a solution to the difficult challenge of thermal management in flexible electronics. For this demonstration, we created thin-film microheaters (serpentine patterns of 10 μm wide wires, covering an area of ca. 250 × 250 μm²) of Ti/Au (300 nm) on PET substrates, and then flowed current through them while monitoring the resistance. The behavior of three different structures were compared: one with the microheater exposed to air, another with a uniform coating (600 nm thick) of poly(methylmethacrylate) (PMMA; Microchem Corp.), and a third with a printed platelet of μs-UNCD (800 × 800 μm²; 400 nm thick). Figure 4a–c correspond to the uncoated, the PMMA, and the μs-UNCD cases, respectively, for applied powers of 53 mW, 97 mW, and 160 mW. The PET substrate (~75 μm) could be easily damaged by heat generated by the microheater. The first stage of thermal degradation occurred at temperatures close to the melting point of 260 °C, followed by a second stage characterized by weight loss at around 350 °C.^[28,29] Stresses associated with differential thermal expansion can also contribute to failure. The images clearly

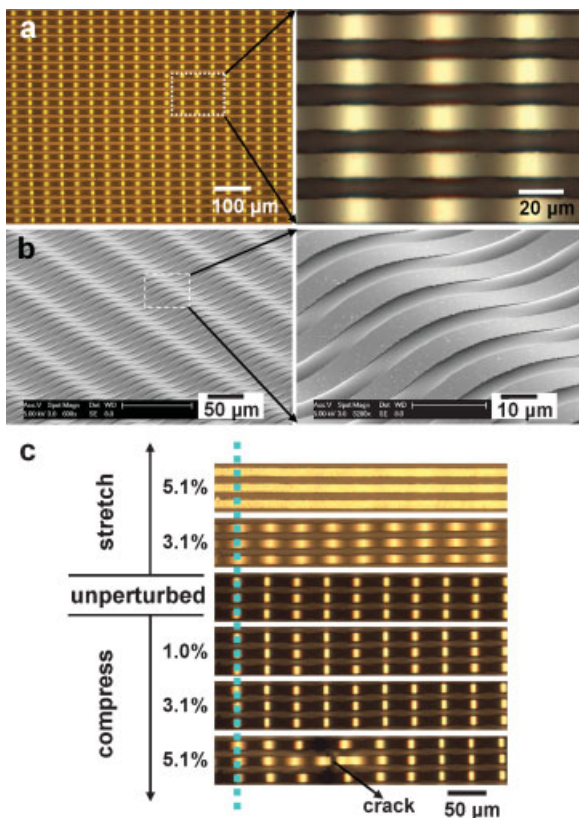


Figure 3. “Wavy” diamond ribbons on a rubber substrate. a) Optical microscopy images of wavy diamond ribbons on PDMS. b) Angled-view SEM images of wavy diamond ribbons from the array shown in (a). c) Optical images of wavy diamond ribbons on PDMS under different applied strains: -5.1% , -3.1% , -1.0% , 3.1% , and 5.1% from the unperturbed state, evaluated along the lengths of the ribbons.

show that the sample with μs -UNCD exhibits the most robust behavior to heating, indicating its effectiveness in heat spreading.

Figure 4d presents the average temperature of the microheaters for the three different cases, as a function of applied power. The temperatures were computed from the known temperature dependence of the resistivity of the metal microheater, according to

$$R(T) = R_a[1 + TCR_a(T - T_a)], \quad (2)$$

where R_a and TCR_a are the resistance and temperature coefficient of resistance, respectively, evaluated at temperature T_a . The resistance R_a is determined by

$$R_a = \rho_a \frac{L}{A}, \quad (3)$$

where ρ_a is resistivity of gold at T_a , L is length, and A is the cross-sectional area of gold wire. The value of $R(T)$ value is obtained simply by dividing applied voltage (V) by the current

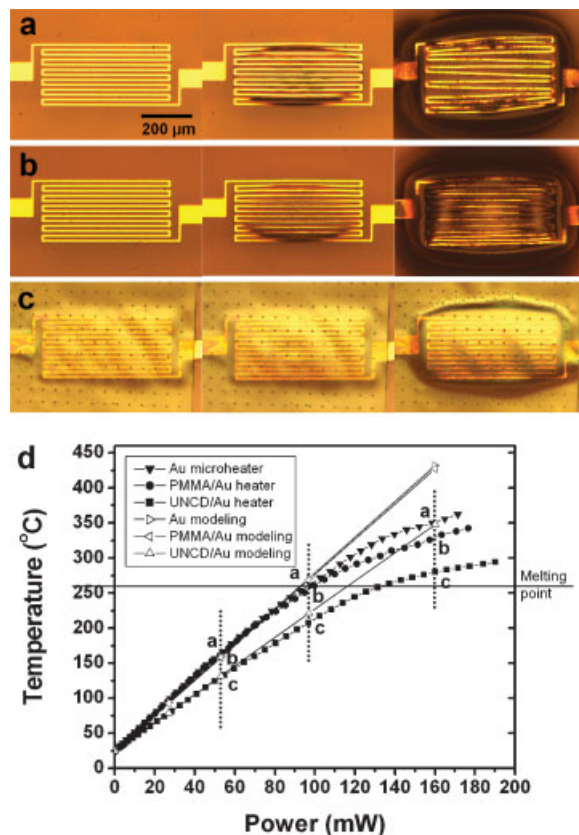


Figure 4. Optical microscopy images of serpentine microheaters on plastic substrates collected at applied powers of 53 mW, 97 mW, and 160 mW, for the case of heaters a) exposed to air, b) coated with a thin (600 nm) spin-cast layer of PMMA, and c) covered with a printed thin (400 nm) platelet of diamond. d) Average heater temperatures from experiment and from finite element modeling as a function of applied power for these three different samples.

(I). Using values of $\rho_{(20^\circ\text{C})}$ and $TCR_{(20^\circ\text{C})}$ for gold of $2.214 \times 10^{-8} \Omega \cdot \text{m}$ and $0.003715^\circ\text{C}^{-1}$ at 20°C , we calculated average temperatures (T) at various applied voltages and currents.^[30–32] The temperatures of the microheater, PMMA/heater, and μs -UNCD/heater systems were, respectively, 261°C , 257°C , and 208°C at a power of 97 mW, and 350°C , 329°C , and 279°C at a power of 160 mW.

Infrared microscopy images of these three systems were collected at different power levels, and are shown in Figure 5. Figure 5a–c correspond to the uncoated, the PMMA and the μs -UNCD cases, respectively, for applied powers of 97 mW and 160 mW. The temperature distribution of the μs -UNCD sample has a rectangular shape with a broad thermal distribution, while the uncoated and PMMA-coated cases show localized heating distributions centered on the gold wires. These distributions illustrate clearly that the UNCD platelet efficiently spreads heat laterally and thereby reduces the peak temperatures. Simple finite-element analysis of the heat flow was conducted to reveal further this behavior. In particular, 2D analysis (COMSOL FEMLab, Multiphysics heat transfer via

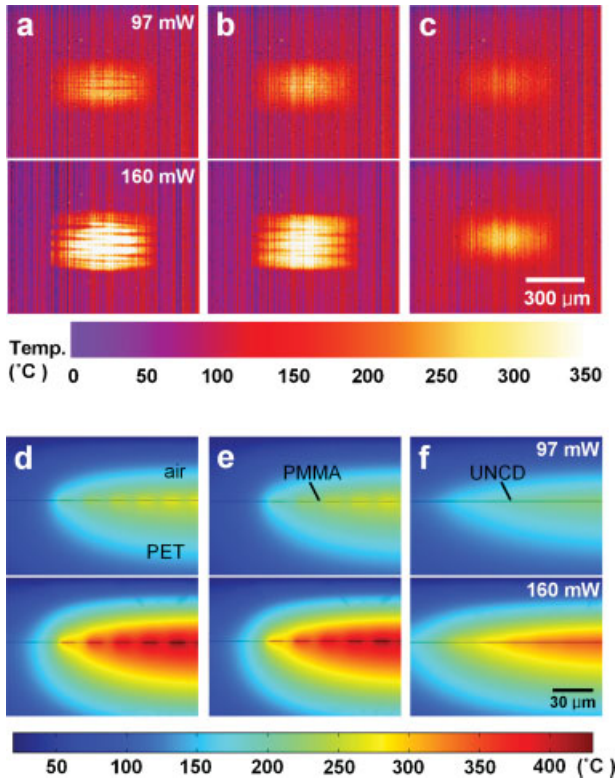


Figure 5. Infrared images of microheaters on PET at various applied powers. a) Au microheater on PET film at 97 mW and 160 mW. b) Au microheater with PMMA top layer at 97 mW and 160 mW. c) Diamond membrane-printed Au microheater at 97 mW and 160 mW. d,e,f) Temperature profiles in cross-section from finite-element analysis at 97 mW and 160 mW.

conduction mode) yields expected temperature distributions for the three systems at different applied powers. The simulated cross-sectional temperature profiles are shown in Figure 5d–f. In the analysis, the gold heater elements supply heat to the system (via Joule heating) which then exits via conduction through the 75 μm PET substrate below the heater and through the PMMA or μs -UNCD coatings, and subsequently through 40 μm of air (i.e., “dead air”) above the structure. The width of the modeled system is ca. 1 mm. For simplicity, convective heat transfer is ignored, and the faces of the PET substrate and the 40 μm air block farthest from the gold heating elements were held at a constant temperature of 25 $^{\circ}\text{C}$. These boundary conditions lead to (maximum) simulated temperatures that vary linearly with the applied power in each system (bare, PMMA-coated, UNCD-coated). The thickness of the air block (40 μm) was chosen to roughly match simulated temperatures of the bare microheater system at low power (<50 mW) to the experimentally measured values, which across that range also vary linearly with applied power. In comparison to simulations of the bare heater, in which the gold is exposed directly to air (thermal conductivity 0.025 W mK^{-1}), simulations of the coated heaters produced lower (maximum) temperatures. Simulations of heaters coated with PMMA (thermal conductivity =

0.15 W mK^{-1}) produced only slightly lower temperatures, but simulations with UNCD (thermal conductivity = 25 W mK^{-1}) produced a more significant temperature reduction and a broader, more uniform temperature profile.^[33] The simulated (maximum) temperatures of the bare microheater, PMMA/heater, and UNCD/heater were 271 $^{\circ}\text{C}$, 269 $^{\circ}\text{C}$, and 221 $^{\circ}\text{C}$ for the applied power of 97 mW, and 432 $^{\circ}\text{C}$, 427.5 $^{\circ}\text{C}$, and 348 $^{\circ}\text{C}$ for the applied power of 160 mW, respectively, as shown in Figure 4d. Simulated temperatures follow the experimental trend closely at low values of applied power (<100 mW for bare and PMMA-coated systems; <80 mW for the UNCD system, Fig. 4d). At higher powers and temperatures, the simulations overestimate the temperature in each system, possibly owing to nonlinear heat transfer mechanisms (e.g., convection, temperature-dependent thermal conductivity of the PET substrate) that were ignored in the simulations.^[34] Despite the discrepancy at higher values of applied power, both the simple simulations and measurements demonstrate that printed UNCD thin films might serve as effective temperature spreaders.

In summary, etching and printing procedures can be used to manipulate thin film microstructures of diamond in a way that allows integration with substrates (e.g., plastic) and creation of structural forms (e.g., bent or wavy) that are incompatible with conventional processing. The resulting capabilities could be useful for certain applications, such as those in thermal management for plastic electronics. Although fine-grained UNCD has been used in this work as an effective example, for more robust applications thicker films of larger grain size material (i.e., high thermal conductivities) can also be used, trading flexibility for even greater thermal performance. Many other immediate benefits of heterogeneous integration are imagined. For instance thin platelets of UNCD co-integrated with high-performance radiofrequency (RF) electronics via transfer printing would enable the monolithic integration of UNCD RF MEMS devices with Si-, GaAs-, or GaN-based drive electronics.^[35] These and other possibilities appear interesting for further study.

Experimental

Preparation of Diamond Microstructures: After growth of the UNCD, a SiO_2 layer (300 nm thick) was deposited by plasma-enhanced chemical vapor deposition (PECVD) using SiH_4 and N_2O at 250 $^{\circ}\text{C}$. Photolithography with AZ 5214 defined a pattern of photoresist (PR) on the surface of the SiO_2 (300 nm)/UNCD (400 nm)/ SiO_2 (1 μm)/Si substrate. The PR served as a mask for RIE etching of the PECVD SiO_2 layer with a CF_4 plasma (Plasmatherm RIE system, 40 sccm CF_4 flow with a chamber base pressure of 50 mTorr (1 Torr = 1.333×10^2 Pa), 100 W RF power for 15 min 30 s). The exposed regions of the UNCD were then etched with an O_2 plasma (chamber pressure of 40 mTorr, 20 sccm O_2 flow, and 220 W RF power for 35 min). Finally, the buried SiO_2 and PECVD SiO_2 layers were then removed in concentrated hydrofluoric acid (HF 49%), and the substrate was washed with de-ionized (DI) water. The etching times were carefully controlled to complete the undercut etching of the UNCD in desired locations, but not in the regions of the anchors, as illustrated in Figure 1.

Transfer Printing: Stamps of poly(dimethylsiloxane) (PDMS; Sylgard 184, Dow Corning) were formed by casting and curing in polystyrene Petri dishes, and then cutting to convenient dimensions. Laminating such stamps against processed μs -UNCD substrates and then quickly peeling them back lifted the μs -UNCD onto the surface of the stamp. Contacting these "inked" stamps against a receiving substrate and then slowly peeling them back transferred the μs -UNCD to the receiver. In certain cases, this transfer was facilitated either by the application of a small shear force to the stamp while in contact with the receiver or by use of a separate adhesion layer.

Preparation of Wavy Diamond Ribbons: After creating μs -UNCD ribbons according to the process of Figure 1, thin layers of Cr (3 nm thick) and SiO_2 (30 nm thick) were deposited by electron beam evaporation (Temescal, Inc). We found empirically that the Cr enhanced the adhesion between the μs -UNCD and SiO_2 . A flat sheet of PDMS (ca. 3 mm thick) was exposed to ultraviolet light in air to create a hydrophilic surface ($-\text{OH}$ and $-\text{O}-\text{Si}-\text{O}-$ end groups) [24], that can provide the strong bonding with the SiO_2/Cr coated μs -UNCD. Other approaches to bond materials to diamond are also possible, including the use of O_2 plasma treatment of the diamond itself [36]. Plasma polymerization represents another possibility [37]. Heating the surface-modified PDMS substrate in a convection oven generated prestrain by thermal expansion. The coefficients of thermal expansion, α , are $3.1 \times 10^{-4} \text{ K}^{-1}$ and $1.2 \times 10^{-6} \text{ K}^{-1}$ for PDMS substrate and UNCD, respectively. The thermally induced prestrain, ε_{pre} , for samples heated to 180°C was calculated by

$$\varepsilon_{\text{pre}} = \Delta\alpha \times \Delta T$$

$$= (3.1 \times 10^{-4} - 1.2 \times 10^{-6}) \times (180 - 25) = 4.8\% \quad (4)$$

The prestrained PDMS was brought into conformal contact with the μs -UNCD ribbons, and then peeled back to leave the ribbons adhered to the PDMS. Subsequent heating in a convection oven led to strong adhesion between ribbons and the PDMS. Finally, the sample was cooled to room temperature (25°C) to release the thermally induced prestrain, thereby creating the wavy μs -UNCD via a nonlinear buckling process.

Fabrication of Au Microheaters: Photolithography with AZ nLOF 2020 for negative imaging defined a pattern of resist on a sheet of PET (75 μm thick). A uniform bilayer of $\text{Ti}(3 \text{ nm})/\text{Au}(300 \text{ nm})$ was then deposited by electron beam evaporation (Temescal, Inc.). Removal of the photoresist by acetone followed by washing with water completed the fabrication of the microheaters. A thin (300 nm), spin-cast layer of BCB was used to planarize the heater structure, and then the μs -UNCD platelets were printed on top. After printing, the samples were placed on a hot plate at 100°C for 10 min, and then in an oven at 75°C for 24 h to cure the BCB. In other samples, PMMA A6 (Microchem Corp.) was spin-coated on top of Au microheater at 2000 rpm for 45 s to produce PMMA layer of 600 nm thickness, and placed in an oven at 75°C for 8 h for removing solvent.

Received: September 26, 2007

Revised: December 18, 2007

Published online: May 5, 2008

- [1] J. Isberg, J. Hammersberg, E. Johnsson, T. Wikstrom, D. J. Twitchen, A. J. Whitehead, S. E. Coe, G. A. Scarsbrook, *Science* **2002**, 297, 1670.
 [2] A. De Sio, J. Achard, A. Tallaire, R. S. Sussmann, A. T. Collins, F. Silva, E. Pace, *Appl. Phys. Lett.* **2005**, 86, 213504.
 [3] H. Masuda, K. Yasui, M. Watanabe, K. Nishio, T. N. Rao, A. Fujishima, *Chem. Lett.* **2000**, 1112.
 [4] S. Srinivasan, J. Hiller, B. Kabius, O. Auciello, *Appl. Phys. Lett.* **2007**, 90, 134101.
 [5] Y. Fu, H. Du, J. Miao, *J. Mater. Process. Technol.* **2003**, 132, 73.

- [6] F. Piazza, D. Grambole, D. Schneider, C. Casiraghi, A. C. Ferrari, J. Robertson, *Diamond Relat. Mater.* **2005**, 14, 994.
 [7] A. Harkonen, S. Suomalainen, E. Saarinen, L. Orsila, R. Koskinen, O. Okhotnikov, S. Calvez, M. Dawson, *Electron. Lett.* **2006**, 42, 693.
 [8] Y. D. Kim, W. Choi, H. Wakimoto, S. Usami, H. Tomokage, T. Ando, *Appl. Phys. Lett.* **1999**, 75, 3219.
 [9] Y. Zhao, B. Zhang, N. Yao, G. Sun, J. Li, *Diamond Relat. Mater.* **2007**, 16, 650.
 [10] S. T. Patton, B. Bhushan, *IEEE Trans. Magn.* **1998**, 34, 575.
 [11] W. I. Urruchi, M. Massi, H. S. Maciel, C. Otani, L. N. Nishioka, *Diamond Relat. Mater.* **2000**, 9, 685.
 [12] R. Abbaschian, H. Zhu, C. Clarke, *Diamond Relat. Mater.* **2005**, 14, 1916.
 [13] J. Laimer, H. Pauser, H. Störi, R. Haubner, B. Lux, *Diamond Relat. Mater.* **1997**, 6, 406.
 [14] D. M. Gruen, *Annu. Rev. Mater. Sci.* **1999**, 29, 211.
 [15] J. A. Carlisle, O. Auciello, *Electrochem. Soc. Interface* **2003**, 12, 28.
 [16] O. Auciello, J. Birrell, J. A. Carlisle, J. Gerbi, X. Xiao, B. Peng, H. Espinosa, *J. Phys. Condens. Matter* **2004**, 16, R539.
 [17] K. J. Hsia, Y. Huang, E. Menard, J.-U. Park, W. Zhou, J. A. Rogers, J. M. Fulton, *Appl. Phys. Lett.* **2005**, 86, 154106.
 [18] M. A. Meitl, X. Feng, J. Y. Dong, E. Menard, P. M. Ferreira, Y. Huang, J. A. Rogers, *Appl. Phys. Lett.* **2007**, 90, 083110.
 [19] S.-H. Hur, D.-Y. Khang, C. Kocabas, J. A. Rogers, *Appl. Phys. Lett.* **2004**, 85, 5730.
 [20] J.-H. Choi, D. Kim, P. J. Yoo, H. H. Lee, *Adv. Mater.* **2005**, 17, 166.
 [21] M. A. Meitl, Z. T. Zhu, V. Kumar, K. J. Lee, X. Feng, Y. Y. Huang, I. Adesida, R. G. Nuzzo, J. A. Rogers, *Nat. Mater.* **2006**, 5, 33.
 [22] A. V. Sumant, D. S. Grierson, J. E. Gerbi, J. Birrell, U. D. Lanke, O. Auciello, J. A. Carlisle, R. W. Carpick, *Adv. Mater.* **2005**, 17, 1040.
 [23] D.-Y. Khang, H. Jiang, Y. Huang, J. A. Rogers, *Science* **2006**, 311, 208.
 [24] Y. Sun, W. M. Choi, H. Jiang, Y. Y. Huang, J. A. Rogers, *Nat. Nanotechnol.* **2006**, 1, 201.
 [25] a) T. Buma, M. Spisar, M. O'Donnell, *Appl. Phys. Lett.* **2001**, 79, 548.
 b) Y. Gurbuz, O. Esame, I. Tekin, W. P. Kang, J. L. Davidson, *Solid-State Electron.* **2005**, 49, 1055.
 [26] a) Y. Sun, V. Kumar, I. Adesida, J. A. Rogers, *Adv. Mater.* **2006**, 18, 2857. b) H. Jiang, D.-Y. Khang, J. Song, Y. Sun, Y. Huang, J. A. Rogers, *Proc. Natl. Acad. Sci. USA* **2007**, 104, 15607.
 [27] H. Jiang, D.-Y. Khang, H. Fei, H. Kim, Y. Huang, J. Xiao, J. A. Rogers, *J. Mech. Phys. Sol.*, in press.
 [28] H. A. Lecomte, J. J. Liggat, *Polym. Degrad. Stab.* **2006**, 91, 681.
 [29] M. T. Freire, A. P. Damant, L. Castle, F. G. R. Reyes, *Packag. Technol. Sci.* **1999**, 12, 29.
 [30] A. Scorzoni, M. Baroncini, P. Placidi, *Sens. Actuators A* **2004**, 116, 137.
 [31] Y. S. Kim, *Sens. Actuators B* **2006**, 114, 410.
 [32] A. G. Bishay, W. Fikry, H. Hunter, H. F. Ragie, *J. Phys. D* **2000**, 33, 2218.
 [33] S. Ahmed, R. Liske, T. Wunderer, M. Leonhardt, R. Ziervogel, C. Fansler, T. Grotjohn, J. Asmussem, T. Schuelke, *Diamond Relat. Mater.* **2006**, 15, 389.
 [34] C. M. A. Lopes, M. I. Felisberti, *Polym. Test.* **2004**, 23, 637.
 [35] S. P. Pacheco, P. Zurcher, S. R. Young, D. Weston, W. J. Dauksher, O. Auciello, J. A. Carlisle, N. Kane, J. P. Birrell, in: *Proc. Gallium Arsenide and Other Semiconductor Application Symp.*, Paris, France **2005**, pp. 577–580.
 [36] E. M. Liston, L. Martinu, M. R. Wertheimer, *Plasma Surface Modification of Polymers: Relevance to Adhesion*, VSP, Utrecht, The Netherlands **1994**, p. 17.
 [37] Y.-B. Guo, F. C.-N. Hong, *Diamond Relat. Mater.* **2003**, 12, 946.